Biophysical Journal Volume 71 November 1996 2802–2814

Vibrational Analysis of Nucleic Acids. V. Force Field and Conformation-Dependent Modes of the Phosphodiester Backbone Modeled by Diethyl Phosphate

Yifu Guan and George J. Thomas, Jr.
Division of Cell Biology and Biophysics, School of Biological Sciences, University of Missouri-Kansas City, Kansas City, MO 64110 USA

ABSTRACT A generalized valence force field is derived for the diethyl phosphate anion [$(CH_3CH_2O)_2PO_2^-$] and its deuterium [$(CH_3CD_2O)_2PO_2^-$, $(CD_3CH_2O)_2PO_2^-$ and $(CD_3CD_2O)_2PO_2^-$] and carbon-13 [$(CH_3{}^{13}CH_2O)_2PO_2^-$] derivatives in the stable *trans-gauche-gauche-trans* conformation. Normal coordinate analysis of the *trans-gauche-gauche-trans* conformer, which serves as a structural analog of the nucleic acid phosphodiester group, is based on comprehensive infrared and Raman spectroscopic data and vibrational assignments obtained for the diethyl phosphate anion. The generalized valence force field is in good agreement with the scaled ab initio force field of diethyl phosphate and represents significant improvement over earlier modeling of the phosphodiester moiety with dimethyl phosphate. The conformational dependence of skeletal C—C—O—P(O_2^-)—O—C—C stretching vibrations is also explored. Starting with the *trans-gauche-gauche-trans* conformation, the frequency dependence of skeletal stretching modes has been obtained by stepwise rotation of the torsion angles of the P—O and C—O bonds corresponding to nucleic acid torsions α (P—O5′), β (O5′—C5′), ϵ (C3′—O3′), and ζ (O3′—P). Both symmetric and antisymmetric phosphoester stretching modes are highly sensitive to P—O and C—O torsions, whereas symmetric and antisymmetric phosphodioxy (PO_2^-) stretching modes are less sensitive. The present results provide an improved structural basis for understanding previously developed empirical correlations between vibrational marker bands and nucleic acid backbone conformation.

INTRODUCTION

Investigations of nucleic acid conformation by Raman and infrared spectroscopy have benefited greatly from studies conducted of oligonucleotide crystals of known three-dimensional structure. (For a recent review, see Thomas and Tsuboi, 1993.) The crystal studies provide an empirical basis for correlating spectral band frequencies and intensities with specific conformational states of DNA and RNA. In favorable cases, Raman band polarizations can also be correlated with nucleic acid structure (Benevides et al., 1993; Thomas et al., 1995; Terpstra et al., 1995). Among the most sensitive vibrational markers of nucleic acid conformation are Raman bands assigned to stretching vibrations localized in the phosphodiester moiety (Erfurth et al., 1972; Thomas et al., 1986). Unfortunately, however, a detailed description of the vibrational modes that give rise to these Raman marker bands has not yet been developed. In particular, the specific internal coordinates on which the vibrational frequencies depend are not known. To determine the relevant internal coordinates and generally to improve understanding of empirically developed spectra-structure correlations of DNA and RNA, we have carried out normal mode and ab initio analyses of simple dialkyl analogs of the nucleic acid phosphodiester group.

Received for publication 24 June 1996 and in final form 23 August 1996.

Address reprint requests to Dr. George J. Thomas, Jr., Division of Cell Biology and Biophysics, School of Biological Sciences, BSB 405, University of Missouri—Kansas City, 5100 Rockhill Road, Kansas City, MO 64110-2499.

0006-3495/96/11/2802/13 $2.00

Previous papers in this series have focused on normal coordinate analyses of ^1H, ^2H and ^{13}C isotopomers of dimethyl phosphate (DMP) (Guan et al., 1994, 1995; Guan and Thomas, 1996a). In the present study we extend the normal coordinate analysis to diethyl phosphate (DEP), which serves as an improved model for the nucleic acid phosphodiester group. The DEP skeleton, C—C—O—P(O_2^-)—O—C—C, which incorporates two C—C valence bonds and two C—C—O—P torsion angles, is expected to provide a better approximation of the vibrational coupling between sugar and phosphate moieties of the nucleic acid backbone. Recently we reported the experimental (infrared and Raman) and calculated (ab initio) vibrational spectra of five DEP isotopomers [$(CH_3CH_2O)_2PO_2^-$ (DEP-h_{10}), $(CH_3CD_2O)_2PO_2^-$ (DEP-d_4), $(CD_3CH_2O)_2PO_2^-$ (DEP-d_6), $(CD_3CD_2O)_2PO_2^-$ (DEP-d_{10}), and $(CH_3{}^{13}CH_2O)_2PO_2^-$ (DEP-$^{13}C_2$)], each in the *trans-gauche-gauche-trans* (*tggt*) conformation (Guan and Thomas, 1996b). The experimental and ab initio spectra were shown to agree closely with each other and to yield reliable vibrational assignments for the five DEP isotopomers.

In the present study we explore the effect of systematic changes in C—C—O—P(O_2^-)—O—C—C conformation on vibrational frequencies of DEP. The approach is as follows. Using recently determined experimental data (Guan and Thomas, 1996b; Guan et al., 1994) and normal mode analysis (Wilson et al., 1955), we develop an empirical generalized valence force field (GVFF) for the crystallographically determined *tggt* conformation of DEP. The present GVFF is tested by comparison with the previously determined ab initio force field (Guan and Thomas, 1996b), as judged by the accuracy of reproduction of vibrational frequencies and potential energy distributions (PEDs) in

spectra of five DEP isotopomers. Agreement between GVFF and ab initio results provides a measure of confidence in the force fields. We then employ the GVFF to calculate key skeletal stretching frequencies, including those of PO_2^-, OPO, C—O, and C—C groups, for conformations of DEP that differ from the *tggt* geometry. The different DEP rotamers have been generated from the initial *tggt* conformation by imposition of independent and stepwise rotations about each of the two phosphoester carbon–oxygen bonds (C—C—O—P torsion angles, designated β and ϵ in Fig. 1) and two phosphorus-oxygen bonds (C—O—P—O torsions, designated α and ζ in Fig. 1).

We find that symmetric and antisymmetric stretching vibrations localized in the OPO moiety are the skeletal modes with the greatest sensitivity to changes in α, β, ϵ, and ζ torsions. Lesser conformational dependencies are exhibited by stretching modes of the PO_2^-, C—O, and C—C groups. The normal coordinate calculations correlate remarkably well with empirical results reported for native and synthetic nucleic acids and oligonucleotides (Thomas and Wang, 1988; Thomas and Tsuboi, 1993). The present findings advance our understanding of the structural basis of conformationally dependent vibrational frequencies in DNA and RNA. The results are discussed in relation to proposed conformation marker bands in infrared and Raman spectra of nucleic acids.

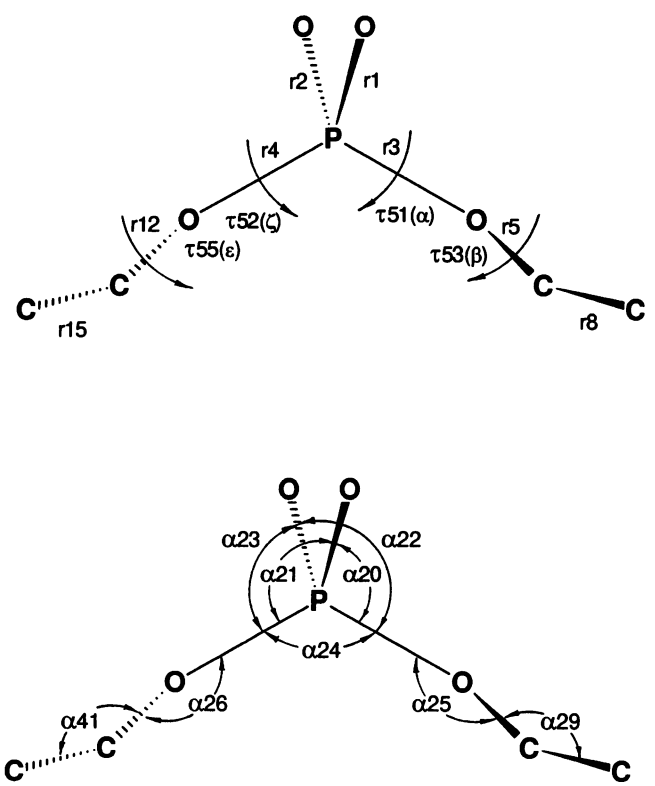

FIGURE 1 Internal coordinates of the DEP anion in the *tggt* conformation. (*Top*) Stretching and torsion coordinates. (*Bottom*) Bending coordinates. For clarity, hydrogen atoms are not shown.

METHODS

Normal coordinate analyses are based on the Wilson **GF**-matrix method (Wilson et al., 1955) and were carried out with the FORTRAN program NCTB (courtesy of Professor Hideo Takeuchi, Pharmaceutical Institute, Tohoku University, Sendai, Japan) on a VAX station 3100 computer (Digital Equipment Corp., Nashua, NH). More-detailed descriptions are given in previous papers of this series (Guan et al., 1994; Guan and Thomas, 1996a).

Normal coordinate calculations for the tggt conformer of DEP

To construct the **G** matrix for DEP in the *tggt* conformation (point group C_2), we employed the x-ray structure of the barium salt (Kyogoku and Iitaka, 1964) with the following average values for bond lengths (Å) and valence and torsion angles (°): P—O = 1.48; P—O = 1.61; C—O = 1.42; C—C = 1.42; C–H = 1.09, ∡O–P–O = 119.9; ∡O–P–O = 102.6; ∡POC = 120.5; ∡OCC = 120.5; ∡OCH = ∡CCH = ∡HCH = 109.5; ∡O—P—O—C = 60; and ∡P—O—C—C = 180. (The notation P—O and P–O indicates phosphooxy and phosphoester valence bonds, respectively.) The 56 internal coordinates and 51 nonredundant symmetry coordinates are given in Fig. 1 and Table 1. To construct the F matrix, we transferred force constants from generalized valence force fields of DMP (Guan et al., 1994) and various ethoxy compounds (Snyder and Zerbi, 1957). Off-diagonal terms corresponding to interactions involving only adjacent internal coordinates were included. Calculated frequencies and assignments based on the PEDs in terms of symmetry coordinates are given for the five isotopomers in Tables 2–6.

Conformational dependence of DEP vibrations

Different rotamers of DEP were generated from the *tggt* conformer by independent and stepwise changes of 30° in each phosphorus–oxygen and carbon–oxygen torsion angle. We constructed each **G** matrix by using the appropriate torsion angles and crystallographic bond lengths and valence angles (Kyogoku and Iitaka, 1964), whereas the **F** matrix was assumed constant. The usual approximation of a single set of bond lengths and valence angles for different rotamers (Wilson et al., 1955) is supported by the virtual invariance of these parameters to changes in phosphoester torsions, as revealed by recent ab initio calculations (Hadzi et al., 1992; Liang et al., 1993). The assumption of a constant **F** matrix throughout the cycle of each torsion angle change is an approximation that is commonly employed in calculations of this type but that cannot be proved (Bicknell-Brown et al., 1982; Taga et al., 1991). However, it is supported by the fact that the torsion angle changes employed here are expected to cause little (<6%) or no change in diagonal force constants and only modest changes (<20%) in off-diagonal constants (Zhao et al., 1990).

For consistency with previous notation (Guan and Thomas, 1995), normal modes representing in-phase and out-of-phase vibrations of equivalent groups of atoms are referred to as symmetric and antisymmetric vibrations, respectively. Eigenvalues of the secular equation $|\mathbf{FG} - \lambda\mathbf{E}| = 0$ determine the normal vibrational frequencies in wavenumber (cm^{-1}) units. Assignments are based on the calculated PEDs in terms of symmetry coordinates. As the PED values for a given vibrational mode do not change appreciably with conformation, we used the frequency exhibiting the most similar set of PED values to construct the corresponding contour map (plot of vibrational frequency versus torsion angle).

RESULTS AND DISCUSSION

Normal modes of *tggt* DEP

Table 2 lists the calculated vibrational frequencies (column 1) and PED values (column 2) of DEP-h_{10} in the *tggt*

TABLE 1 Symmetry coordinates of diethyl phosphate

Symmetry coordinate	Description
A Species	
S1 = $r1 + r2$	$\nu_s(PO_2^-)$
S2 = $r3 + r4$	$\nu_s(OPO)$
S3 = $r5 + r12$	$\nu_s(CO)$
S4 = $r8 + r15$	$\nu_s(CC)$
S5 = $r6 + r7 + (r13 + r14)$	$\nu_s(CH_2)$
S6 = $r6 - r7 + (r13 - r14)$	$\nu_a(CH_2)$
S7 = $r9 + r10 + r11 + (r16 + r17 + r18)$	$\nu_s(CH_3)$
S8 = $2r9 - r10 - r11 + (2r16 - r17 - r18)$	$\nu_a(CH_3)$
S9 = $r10 - r11 + r17 - r18$	$\nu_a(CH_3)$
S10 = $\alpha 19$	$\delta(PO_2^-)$
S11 = $\alpha 24$	$\delta(OPO)$
S12 = $\alpha 20 - \alpha 21 - \alpha 22 + \alpha 23$	$t(PO_2^-)$
S13 = $\alpha 25 + \alpha 26$	$\delta_s(POC)$
S14 = $5\alpha 29 - \alpha 30 - \alpha 27 - \alpha 28 - \alpha 31 - \alpha 32 + (5\alpha 41 - \alpha 42 - \alpha 39 - \alpha 40 - \alpha 43 - \alpha 44)$	$\delta_s(OCC)$
S15 = $4\alpha 30 - \alpha 27 - \alpha 28 - \alpha 31 - \alpha 32 + (4\alpha 42 - \alpha 39 - \alpha 40 - \alpha 43 - \alpha 44)$	$\delta(CH_2)$
S16 = $\alpha 27 - \alpha 28 - \alpha 31 + \alpha 32 + (\alpha 39 - \alpha 40 - \alpha 43 + \alpha 44)$	$t(CH_2)$
S17 = $\alpha 27 + \alpha 28 - \alpha 31 - \alpha 32 + (\alpha 39 + \alpha 40 - \alpha 43 - \alpha 44)$	$\omega(CH_2)$
S18 = $\alpha 27 - \alpha 28 + \alpha 31 - \alpha 32 + (\alpha 39 - \alpha 40 + \alpha 43 - \alpha 44)$	$r(CH_2)$
S19 = $\alpha 33 + \alpha 34 + \alpha 35 - \alpha 36 - \alpha 37 - \alpha 38 + (\alpha 45 + \alpha 46 + \alpha 47 - \alpha 48 - \alpha 49 - \alpha 50)$	$\delta_s(CH_3)$
S20 = $-\alpha 36 - \alpha 37 + 2\alpha 38 + (-\alpha 48 - \alpha 49 + 2\alpha 50)$	$\delta_a(CH_3)$
S21 = $\alpha 36 - \alpha 37 + \alpha 48 - \alpha 49$	$\delta_a(CH_3)$
S22 = $2\alpha 33 - \alpha 34 - \alpha 35 + (2\alpha 45 - \alpha 46 - \alpha 47)$	$r(CH_3)$
S23 = $\alpha 34 - \alpha 35 + (\alpha 46 - \alpha 47)$	$r(CH_3)$
S24 = $\tau 51 + \tau 52$	$\tau_s(OPOC)$
S25 = $\tau 53 + \tau 55$	$\tau_s(POCC)$
S26 = $\tau 54 + \tau 56$	$\tau_s(OCCH)$
B Species	
S1 = $r1 - r2$	$\nu_a(PO_2^-)$
S2 = $r3 - r4$	$\nu_a(OPO)$
S3 = $r5 - r12$	$\nu_a(CO)$
S4 = $r8 - r15$	$\nu_a(CC)$
S5 = $r6 + r7 - (r13 + r14)$	$\nu_s(CH_2)$
S6 = $r6 - r7 - (r13 - r14)$	$\nu_a(CH_2)$
S7 = $r9 + r10 + r11 - (r16 + r17 + r18)$	$\nu_s(CH_3)$
S8 = $2r9 - r10 - r11 - (2r16 - r17 - r18)$	$\nu_a(CH_3)$
S9 = $r10 - r11 - (r17 - r18)$	$\nu_a(CH_3)$
S10 = $\alpha 20 + \alpha 21 - \alpha 22 - \alpha 23$	$r(PO_2^-)$
S11 = $\alpha 20 - \alpha 21 + \alpha 22 - \alpha 23$	$\omega(PO_2^-)$
S12 = $\alpha 25 - \alpha 26$	$\delta_a(POC)$
S13 = $5\alpha 29 - \alpha 30 - \alpha 27 - \alpha 28 - \alpha 31 - \alpha 32 - (5\alpha 41 - \alpha 42 - \alpha 39 - \alpha 40 - \alpha 43 - \alpha 44)$	$\delta_a(OCC)$
S14 = $4\alpha 30 - \alpha 27 - \alpha 28 - \alpha 31 - \alpha 32 - (4\alpha 42 - \alpha 39 - \alpha 40 - \alpha 43 - \alpha 44)$	$\delta(CH_2)$
S15 = $\alpha 27 - \alpha 28 - \alpha 31 + \alpha 32 - (\alpha 39 - \alpha 40 - \alpha 43 + \alpha 44)$	$t(CH_2)$
S16 = $\alpha 27 + \alpha 28 - \alpha 31 - \alpha 32 - (\alpha 39 + \alpha 40 - \alpha 43 - \alpha 44)$	$\omega(CH_2)$
S17 = $\alpha 27 - \alpha 28 + \alpha 31 - \alpha 32 - (\alpha 39 - \alpha 40 + \alpha 43 - \alpha 44)$	$r(CH_2)$
S18 = $\alpha 33 + \alpha 34 + \alpha 35 - \alpha 36 - \alpha 37 - \alpha 38 - (\alpha 45 + \alpha 46 + \alpha 47 - \alpha 48 - \alpha 49 - \alpha 50)$	$\delta_s(CH_3)$
S19 = $-\alpha 36 - \alpha 37 + 2\alpha 38 - (-\alpha 48 - \alpha 49 + 2\alpha 50)$	$\delta_a(CH_3)$
S20 = $\alpha 36 - \alpha 37 - (\alpha 48 - \alpha 49)$	$\delta_a(CH_3)$
S21 = $2\alpha 33 - \alpha 34 - \alpha 35 - (2\alpha 45 - \alpha 46 - \alpha 47)$	$r(CH_3)$
S22 = $\alpha 34 - \alpha 35 - (\alpha 46 - \alpha 47)$	$r(CH_3)$
S23 = $\tau 51 - \tau 52$	$\tau_a(OPOC)$
S24 = $\tau 53 - \tau 55$	$\tau_a(POCC)$
S25 = $\tau 54 - \tau 56$	$\tau_a(OCCH)$

Symmetry coordinates are unnormalized. Internal coordinates are defined in Fig. 1. Symbols and abbreviations: ν, stretch; δ, bend; ω, wag; r, rock; t, twist; τ, torsion; s, symmetric; a, antisymmetric.

conformation. Experimental frequencies (column 3) and empirical assignments (column 4) are included for comparison. Analogous listings are given for DEP-$^{13}C_2$ (Table 3), DEP-d_4 (Table 4), DEP-d_6 (Table 5), and DEP-d_{10} (Table 6). Within each table the calculated and experimental frequencies are in good agreement with one another; the PED values and empirical assignments also agree satisfactorily and are consistent with observed isotope effects (Fig. 2). As expected, ^{13}C-substitution of methylene carbons introduces only small frequency shifts (cf. Tables 2 and 3), whereas ^{2}H-substitution causes many large shifts (cf. Tables 2 and 4–6). The latter shifts indicate significantly different cou-

TABLE 2 Calculated and experimental frequencies of DEP-h_{10}

Calculated Frequency	Calculated PED (%)	Experimental Frequency	Empirical Assignment
2998	$\nu_a(CH_3)$ 99	2981	$\nu_a(CH_3)$
2998	$\nu_a(CH_3)$ 99		
2957	$\nu_a(CH_2)$ 100	2952	$\nu_a(CH_2)$
2929	$\nu_s(CH_3)$ 99	2936	$\nu_s(CH_3)$
2896	$\nu_s(CH_2)$ 100	2901	$\nu_s(CH_2)$
1495	$\delta(CH_2)$ 96	1486	$\delta(CH_2)$
1452	$\delta_a(CH_3)$ 81	1460	$\delta_a(CH_3)$
1450	$\delta_a(CH_3)$ 92	1444	$\delta_a(CH_3)$
1403	$\omega(CH_2)$ 82, $\delta_s(CH_3)$ 10	1391	$\omega(CH_2)$
1360	$\delta_s(CH_3)$ 84, $\nu_s(CC)$ 10	1364	$\delta_s(CH_3)$
1259	$t(CH_2)$ 77, $r(CH_3)$ 11	1280	$t(CH_2)$
1239	$\nu_a(PO_2^-)$ 97	1236	$\nu_a(PO_2^-)$
1186	$r(CH_2)$ 53, $r(CH_3)$ 23	1159	$r(CH_2)$, $r(CH_3)$
1113	$r(CH_3)$ 43, $\nu_s(CO)$ 32, $\delta_s(OCC)$ 14	1115	$r(CH_3)$
1092	$\nu_s(PO_2^-)$ 98	1093	$\nu_s(PO_2^-)$
1080	$\nu_s(CO)$ 37, $\nu_s(CC)$ 37, $\nu_s(PO_2^-)$ 12	1075	$\nu_s(CO)$
1055	$\nu_a(CO)$ 48, $\nu_a(CC)$ 35, $\nu_a(OPO)$ 12	1048	$\nu_a(CO)$
954	$\nu_a(CC)$ 35, $\nu_a(OPO)$ 37, $\nu_a(CO)$ 11	954	$\nu_a(CC)$
948	$\nu_s(CC)$ 42, $\nu_s(OPO)$ 27, $r(CH_3)$ 12	938	$\nu_s(CC)$
794	$\nu_a(OPO)$ 38, $\nu_a(CO)$ 33, $r(CH_3)$ 18	806	$\nu_a(OPO)$
790	$r(CH_3)$ 57, $r(CH_2)$ 35	798	$r(CH_2)$, $r(CH_3)$
774	$\nu_s(OPO)$ 43, $\nu_a(CO)$ 31, $r(CH_2)$ 22	753	$\nu_s(OPO)$
549	$\omega(PO_2^-)$ 56, $r(PO_2^-)$ 21, $\delta_a(OCC)$ 10	563	$r(PO_2^-)$
515	$\delta(PO_2^-)$ 50, $\delta(OPO)$ 31, $\delta_a(OCC)$ 10	549	$\delta(PO_2^-)$
474	$r(PO_2^-)$ 50, $\delta_a(OCC)$ 31, $\nu_a(CO)$ 18	497	$\omega(PO_2^-)$
398	$t(PO_2^-)$ 59, $\delta(OPO)$ 16, $\delta(PO_2^-)$ 10	390	$t(PO_2^-)$
366	$\delta_s(OCC)$ 52, $\delta(OPO)$ 29, $t(PO_2^-)$ 10	351	$\delta(OPO)$
336	$\delta_a(OCC)$ 45, $\nu_a(OPO)$ 24, $\omega(PO_2^-)$ 16	(320)	$\delta_s(OCC)$
328	$\delta(PO_2^-)$ 33, $\delta_s(OCC)$ 16, $\nu_s(OPO)$ 16		
184	$\tau_a(P—O)$ 66, $\tau_a(C—C)$ 14, $\delta_a(POC)$ 13		
162	$\delta_s(POC)$ 64, $\tau_a(P—O)$ 14, $r(PO_2^-)$ 12	(189)	$\delta(POC)$
149	$\delta_a(POC)$ 62, $\omega(PO_2^-)$ 13		
129	$\tau_s(C—C)$ 66, $\tau_a(P—O)$ 14	(128)	$\tau(P—O)$
113	$\tau_a(C—C)$ 81, $\tau_a(P—O)$ 13		
87	$\tau_s(P—O)$ 64, $t_s(C—C)$ 24		
60	$\tau_a(O—C)$ 92	(56)	$\tau(O—C)$
43	$\tau_s(O—C)$ 84		

Calculated frequencies are in wavenumber (cm^{-1}) units. Experimental frequencies are from Raman spectra. Frequencies in parentheses are those of Taga et al. (1991) but were not used for refining the force field. For calculated PEDs, only contributions larger than 10% are listed. Symmetry coordinates are defined in Table 1. Notation and abbreviations for empirical assignments are given in Table 1.

TABLE 3 Calculated and experimental frequencies of DEP-$^{13}C_2$

Calculated Frequency	Calculated PED (%)	Experimental Frequency	Empirical Assignment
2978	$\nu_a(CH_3)$ 94	2979	$\nu_a(CH_3)$
2976	$\nu_a(CH_3)$ 78		
2950	$\nu_a(^{13}CH_2)$ 96	2918	$\nu_a(^{13}CH_2)$
2930	$\nu_s(CH_3)$ 90	2937	$\nu_s(CH_3)$
2898	$\nu_s(^{13}CH_2)$ 91	2894	$\nu_s(^{13}CH_2)$
1484	$\delta(^{13}CH_2)$ 62, $\omega(^{13}CH_2)$ 26	1485	$\delta(^{13}CH_2)$
1449	$\delta_a(CH_3)$ 82	1459	$\delta_a(CH_3)$
1446	$\delta_a(CH_3)$ 88	1443	$\delta_a(CH_3)$
1396	$\omega(^{13}CH_2)$ 90	1391	$\omega(^{13}CH_2)$
1335	$\delta_s(CH_3)$ 84, $\nu_s(^{13}CC)$ 15	1364	$\delta_s(CH_3)$
1303	$t(^{13}CH_2)$ 62, $r(CH_3)$ 18	1285	$t(^{13}CH_2)$
1237	$\nu_a(PO_2^-)$ 87	1235	$\nu_a(PO_2^-)$
1161	$r(^{13}CH_2)$ 34, $r(CH_3)$ 28, $t(^{13}CH_2)$ 28	1145	$r(CH_3)$, $r(^{13}CH_2)$
1113	$r(CH_3)$ 53, $\delta_s(O^{13}CC)$ 12, $\nu_s(^{13}CO)$ 14	1112	$r(CH_3)$
1095	$\nu_s(PO_2^-)$ 87	1084	$\nu_s(PO_2^-)$
1065	$\nu_s(^{13}CO)$ 34, $\nu_s(^{13}CC)$ 28, $\nu_s(PO_2^-)$ 15	1059	$\nu_s(^{13}CO)$
1057	$\nu_a(^{13}CO)$ 37, $\nu_a(OPO)$ 24, $\nu_a(^{13}CC)$ 21	1031	$\nu_a(^{13}CO)$
954	$\nu_a(^{13}CC)$ 39, $\nu_s(OPO)$ 30, $r(CH_3)$ 11	950	$\nu_a(^{13}CC)$
947	$\nu_s(^{13}CC)$ 39, $\nu_s(OPO)$ 19	935	$\nu_s(^{13}CC)$
784	$\nu_a(OPO)$ 34, $\nu_a(^{13}CO)$ 50	802	$\nu_a(OPO)$
787	$r(CH_3)$ 56, $r(^{13}CH_2)$ 35	793	$r(^{13}CH_2)$, $r(CH_3)$
751	$\nu_s(OPO)$ 56, $\nu_a(^{13}CO)$ 32	753	$\nu_s(OPO)$
545	$\omega(PO_2^-)$ 62, $r(PO_2^-)$ 17		
510	$\delta(PO_2^-)$ 54, $\delta(OPO)$ 30		
480	$r(PO_2^-)$ 53, $\omega(PO_2^-)$ 24		
392	$t(PO_2^-)$ 71, $\delta(OPO)$ 10		
365	$\delta(OPO)$ 42, $\delta_a(O^{13}CC)$ 31, $\delta(PO_2^-)$ 10		
324	$\delta_a(O^{13}CC)$ 52, $\nu_a(OPO)$ 14		
319	$\delta_s(O^{13}CC)$ 53, $\nu_s(OPO)$ 13		
263	$\tau_a(^{13}C—C)$ 93		
251	$\tau_s(^{13}C—C)$ 84		
157	$\delta_s(PO^{13}C)$ 70		
150	$\delta_a(PO^{13}C)$ 56, $t(PO_2^-)$ 15		
103	$\tau_a(P—O)$ 65, $r(PO_2^-)$ 16		
76	$\tau_s(P—O)$ 81		
57	$\tau_a(O—^{13}C)$ 87		
37	$\tau_s(O—^{13}C)$ 84		

Notation and abbreviations are given in Table 1.

pling phenomena for protium (^1H) and deuterium (^2H or D) forms of DEP. They are discussed below.

The available spectroscopic data (Guan and Thomas, 1996b) provide a solid basis for developing a comprehensive force field for DEP. Results for DEP-h_{10} and DEP-$^{13}C_2$ were used to establish a preliminary approximation to the force field, subsequently refined by incorporation of results for the deuterated species DEP-d_4, DEP-d_6, and DEP-d_{10}.

As in the case of DMP (Guan et al., 1994, 1995), we incorporated anharmonicities in hydrogen stretching modes of the methyl and methylene groups into the DEP force field by elevating the C-D stretching force constants by 2–3%.

TABLE 4 Calculated and experimental frequencies of DEP-d_4

Calculated Frequency	Calculated PED (%)	Experimental Frequency	Empirical Assignment
2998	$\nu_a(CH_3)$ 99	2980	$\nu_a(CH_3)$
2997	$\nu_a(CH_3)$ 99		
2929	$\nu_s(CH_3)$ 99	2937	$\nu_s(CH_3)$
2207	$\nu_a(CD_2)$ 98	2217	$\nu_a(CD_2)$
2101	$\nu_s(CD_2)$ 100	2124	$\nu_s(CD_2)$
1451	$\delta_a(CH_3)$ 91	1460	$\delta_a(CH_3)$
1449	$\delta_a(CH_3)$ 92	1439	$\delta_a(CH_3)$
1365	$\delta_s(CH_3)$ 98	1377	$\delta_s(CH_3)$
1240	$\nu_a(PO_2^-)$ 97	1237	$\nu_a(PO_2^-)$
1198	$\omega(CD_2)$ 48, ν(CC) 23, ν(CO) 23	1169	$\omega(CD_2)$
1118	$r(CH_3)$ 57, $r(CD_2)$ 18	1138	$\delta(CD_2)$
1099	$\omega(CD_2)$ 45, $\nu_s(PO_2^-)$ 22, ν(CC) 18		
1091	$\nu_s(PO_2^-)$ 79, $r(CH_3)$ 10	1106	$\nu_s(PO_2^-)$
1080	$\delta(CD_2)$ 100	1068	$r(CH_3)$
1009	ν_s(CO) 44, ν_s(OPO) 21, $\omega(CD_2)$ 21	1041	ν_s(CO)
984	ν_a(CO) 48, ν_a(OPO) 28	1008	ν_a(CO)
916	$t(CD_2)$ 62, $r(CD_2)$ 25	920	$t(CD_2)$,ν_a(CC)
886	ν_a(CC) 36, ν_a(OPO) 22, $\omega(CD_2)$ 20	886	ν_a(CC)
884	ν_s(CC) 38, $\omega(CD_2)$ 24, ν_s(OPO) 18	865	ν_s(CC)
782	ν_a(OPO) 32, ν_a(CO) 29, $\omega(CD_2)$ 20	797	ν_a(OPO)
763	ν_s(OPO) 38, ν_s(CO) 29, $r(CH_3)$ 24	751	ν_s(OPO)
670	$r(CD_2)$ 46, $r(CH_3)$ 31, $t(CD_2)$ 17	678	$r(CD_2)$,$r(CH_3)$
543	$\omega(PO_2^-)$ 58, $r(PO_2^-)$ 18, δ_a(OCC) 12		
511	$\delta(PO_2^-)$ 52, δ(OPO) 28, δ_s(OCC) 12		
468	$r(PO_2^-)$ 52, δ_a(OCC) 29, ν_a(CO) 18		
390	$t(PO_2^-)$ 60, δ(OPO) 16, $\delta(PO_2^-)$ 10		
359	δ_s(OCC) 49, δ(OPO) 23, $t(PO_2^-)$ 11		
333	δ_a(OCC) 46, $\omega(PO_2^-)$ 17, ν_a(OPO) 16		
324	$\delta(PO_2^-)$ 31, $t(PO_2^-)$ 22, δ(OPO) 16		
173	τ_a(P—O) 55, δ_a(POC) 23, τ_a(O—C) 13		
156	δ_a(POC) 56, τ_a(P—O) 23, $r(PO_2^-)$ 11		
145	δ_s(POC) 66, $t(PO_2^-)$ 12		
123	τ_s(C—C) 80		
112	τ_a(C—C) 82, τ_a(P—O) 13		
78	τ_s(P—O) 84, τ_s(C—C) 12		
54	τ_a(O—C) 92		
42	τ_s(O—C) 86		

Notation and abbreviations are given in Table 1.

TABLE 5 Calculated and experimental frequencies of DEP-d_6

Calculated Frequency	Calculated PED (%)	Experimental Frequency	Empirical Assignment
2957	$\nu_a(CH_2)$ 99	2959	$\nu_a(CH_2)$
2896	$\nu_s(CH_2)$ 100	2903	$\nu_s(CH_2)$
2241	$\nu_a(CD_3)$ 92	2234	$\nu_a(CD_3)$
2240	$\nu_a(CD_3)$ 92		
2111	$\nu_s(CD_3)$ 97	2072	$\nu_s(CD_3)$
1492	$\delta(CH_2)$ 100	1481	$\delta(CH_2)$
1394	$\omega(CH_2)$ 99	1390	$\omega(CH_2)$
1241	$\nu_a(PO_2^-)$ 65, $t(CH_2)$ 29	1235	$\nu_a(PO_2^-)$
1238	$t(CH_2)$ 88	1270	$t(CH_2)$
1128	$\delta_s(CD_3)$ 41, ν_s(CC) 47	1145	$\delta_s(CD_3)$
1120	$r(CH_2)$ 60, $r(CD_3)$ 13	1086	$r(CH_2)$, $r(CD_3)$
1095	$\nu_s(PO_2^-)$ 84, ν_s(CO) 12	1110	$\nu_s(PO_2^-)$
1080	ν_s(CO) 53, $\nu_s(PO_2^-)$ 19, $\delta_a(CD_3)$ 10	1064	ν_s(CO)
1042	$\delta_a(CD_3)$ 96	1047	$\delta_a(CD_3)$
1040	$\delta_a(CD_3)$ 85, ν_s(CC) 13		
1020	ν_a(CO) 49, $\delta_a(CD_3)$ 34, ν_a(OPO) 10	1025	ν_a(CO)
965	$\delta_s(CD_3)$ 26, δ_s(OCC) 24, $r(CD_3)$ 23	964	$r(CD_3)$
874	ν_a(CC) 25, ν_a(OPO) 32, $\delta_a(CD_3)$ 18	890	ν_a(CC)
871	ν_s(CC) 26, ν_s(OPO) 30, $\delta_a(CD_3)$ 19	863	ν_s(CC)
724	ν_a(OPO) 17, ν_a(CC) 17, $r(CD_3)$ 40	724	ν_a(OPO)
695	ν_s(OPO) 23, ν_s(CO) 21, $r(CD_3)$ 47	690	ν_s(OPO)
646	$r(CD_3)$ 72, $r(CH_2)$ 19	670	$r(CH_2)$, $r(CD_3)$
542	$\omega(PO_2^-)$ 50, $r(PO_2^-)$ 29		
509	$\delta(PO_2^-)$ 51, δ(OPO) 33		
452	$r(PO_2^-)$ 40, δ_a(OCC) 22, ν_a(OC) 20		
397	$t(PO_2^-)$ 55, δ(OPO) 19, $\delta(PO_2^-)$ 11		
348	δ(OPO) 27, $t(PO_2^-)$ 24, δ_s(OCC) 18		
310	δ_a(OCC) 51, ν_a(OPO) 14, $\omega(PO_2^-)$ 11		
306	δ_s(OCC) 53, $\delta(PO_2^-)$ 17, ν_s(OPO) 15		
180	τ_a(P—O) 76		
156	δ_s(POC) 66, $r(PO_2^-)$ 12, δ_a(OCC) 11		
142	δ_s(POC) 66, $t(PO_2^-)$ 12, δ_s(OCC) 10		
113	τ_s(P—O) 43, τ_s(C—C) 39		
84	τ_a(C—C) 81, τ_a(O—C) 11		
69	τ_s(C—C) 57, τ_s(P—O) 38		
53	τ_a(O—C) 84		
38	τ_s(O—C) 85		

Notation and abbreviations are given in Table 1.

The final GVFF, which satisfactorily reproduces vibrational frequencies and PED values for all isotopomers, is given in Table 7.

Phosphorus–oxygen stretching vibrations

For all isotopomers, antisymmetric and symmetric phosphodioxy (PO_2^-) stretching modes are calculated at 1239 ± 2 and 1095 ± 2 cm^{-1}, respectively, in good agreement with observed and ab initio frequencies (Guan and Thomas,

TABLE 6 Calculated and experimental frequencies of DEP-d_{10}

Calculated Frequency	Calculated PED (%)	Experimental Frequency	Empirical Assignment
2241	$\nu_a(CD_3)$ 96	2236	$\nu_a(CD_3)$
2241	$\nu_a(CD_3)$ 95	2230	$\nu_a(CD_3)$
2204	$\nu_a(CD_2)$ 95	2211	$\nu_a(CD_2)$
2111	$\nu_s(CD_3)$ 96	2148	$\nu_s(CD_3)$, $\nu_s(CD_2)$
2102	$\nu_s(CD_2)$ 99	2108	$\nu_s(CD_3)$, $\nu_s(CD_2)$
1240	$\nu_a(PO_2^-)$ 96	1239	$\nu_a(PO_2^-)$
1198	$\omega(CD_2)$ 53, $\nu_s(CC)$ 36	1199	$\omega(CD_2)$, $\delta_s(CD_3)$
1185	$\nu_s(CC)$ 45, $\omega(CD_2)$ 45	1199	$\omega(CD_2)$, $\delta_a(CD_3)$
1098	$\nu_s(PO_2^-)$ 30, $\delta_s(CD_3)$ 39, $\nu_s(CO)$ 18	1122	$\delta_s(CD_3)$, $\omega(CD_2)$
1091	$\nu_s(PO_2^-)$ 72, $\delta_s(CD_3)$ 13	1105	$\nu_s(PO_2^-)$
1085	$\delta_s(CD_3)$ 58, $\delta(CD_2)$ 45	1061	$\delta(CD_2)$, $\delta_a(CD_3)$
1042	$\delta_a(CD_3)$ 97	1053	$\delta_a(CD_3)$, $\delta(CD_2)$
1012	$\nu_s(CO)$ 41, $\delta_s(CD_3)$ 13, $\omega(CD_2)$ 13	1011	$\nu_s(CO)$, $\delta_a(CD_3)$
990	$\nu_a(CO)$ 70, $r(CD_2)$ 10, $\nu_a(OPO)$ 10	1011	$\nu_a(CO)$
984	$r(CD_2)$ 45, $r(CD_3)$ 35	977	$r(CD_3)$, $r(CD_2)$
949	$r(CD_3)$ 27, $\nu_s(OPO)$ 26, $\delta_s(OCC)$ 22	931	$r(CD_3)$, $r(CD_2)$
912	$t(CD_2)$ 75, $r(CD_2)$ 11	910	$t(CD_2)$
840	$\nu_a(CC)$ 25, $\nu_a(OPO)$ 31, $\delta_s(CD_2)$ 15	845	$\nu(CC)$
834	$\nu_s(CC)$ 27, $\nu_s(OPO)$ 27, $\delta_s(CD_2)$ 16	828	$\nu(CC)$
708	$r(CD_3)$ 39, $\nu_a(CO)$ 15	715	$\nu_a(OPO)$
682	$\nu_s(OPO)$ 20, $r(CD_3)$ 45, $\nu_s(CO)$ 19	681	$\nu_s(OPO)$
578	$r(CD_3)$ 66, $r(CD_3)$ 38, $t(CD_2)$ 24		
534	$\omega(PO_2^-)$ 48, $r(PO_2^-)$ 25		
503	$\delta(PO_2^-)$ 54, $\delta(OPO)$ 29		
448	$r(PO_2^-)$ 43, $\delta(OCC)$ 21, $\nu_a(CO)$ 21		
389	$t(PO_2^-)$ 56, $\delta(OPO)$ 20, $\delta(PO_2^-)$ 10		
341	$\delta(OPO)$ 29, $t(PO_2^-)$ 23, $\delta_s(OCC)$ 17		
306	$\delta_a(OCC)$ 52, $\nu(OPO)$ 12, $\omega(PO_2^-)$ 11		
303	$\delta_s(OCC)$ 54, $\delta(OPO)$ 15, $\nu(PO_2^-)$ 16		
168	$\tau_a(P—O)$ 68, $\delta_a(POC)$ 15		
152	$\delta_a(POC)$ 61, $\tau_a(P—O)$ 17		
140	$\delta_s(POC)$ 69, $\pi(PO_2^-)$ 11		
102	$\tau_s(C—C)$ 54, $\tau_s(P—O)$ 34		
83	$\tau_a(C—C)$ 85		
67	$\tau_s(P—O)$ 50, $\tau_s(C—C)$ 43		
49	$\tau_a(O—C)$ 80		
37	$\tau_s(O—C)$ 87		

Notation and abbreviations are given in Table 1.

1996b). As expected, ^{13}C and ^{2}H substitutions do not affect the phosphodioxy stretching modes. Conversely, methyl group deuteration significantly alters stretching modes of the phosphodiester (OPO) group. Antisymmetric and symmetric OPO modes of DEP-h_{10}, DEP-$^{13}C_2$, and DEP-d_4 are observed, respectively, at 801 ± 1 and 760 ± 5 cm^{-1}. Remarkably, the OPO bands, though they are unshifted by methylene deuteration, are shifted to 705 ± 5 and 685 ± 5 cm^{-1}, respectively, in both DEP-d_6 and DEP-d_{10}. Previous ab initio analyses of these DEP isotopomers indicated that the large frequency shifts are due to coupling of OPO stretching modes with CD_3 rocking modes, whereas no significant coupling occurs with CD_2 modes (Guan and Thomas, 1996b). The present normal coordinate calculations support the ab initio results: In DEP-d_6 (Table 5) the calculated antisymmetric (724 cm^{-1}) and symmetric (695 cm^{-1}) OPO stretching modes involve a relatively large contribution (≈40%) from CD_3 rocking.

C—O and C—C stretching vibrations

Symmetric and antisymmetric C—O stretching modes of DEP-h_{10} are calculated at 1080 and 1055 cm^{-1}, respectively, in good agreement with experimental values of 1075 and 1048 cm^{-1} (Table 2). Similarly good agreement occurs for DEP-$^{13}C_2$ (Table 3). Calculated and experimental frequencies are satisfactory for DEP-d_6 and DEP-d_{10}. In the case of DEP-d_4 we assign the bands observed at 1041 and 1008 cm^{-1} to the C—O modes, although the frequencies calculated by normal mode analysis (1009 and 984 cm^{-1}) and ab initio analysis (~1005 cm^{-1}) differ somewhat from experimental values for this isotopomer. The discrepancy may be due to coupling effects not accounted for by the calculations.

Two C—C stretching modes are calculated at 954 and 948 cm^{-1}, close to the experimental values of 954 and 938 cm^{-1} (Table 2). Corresponding modes are calculated near 885 cm^{-1} for DEP-d_4 (Table 4), 872 cm^{-1} for DEP-d_6 (Table 5), and 837 cm^{-1} for DEP-d_{10} (Table 6), reflecting the shifts to lower frequency expected with deuteration. In each case the calculated and observed frequencies are in good agreement, although the corresponding PED values demonstrate notable differences in the internal coordinates (Tables 2–6). Thus, C—C stretching modes couple differently with CD_2 and CD_3 deformation modes in the differently deuterated species.

CH_2 scissoring and wagging vibrations

CH_2 scissoring and wagging modes are calculated at 1495 and 1403 cm^{-1} in DEP-h_{10} and at 1492 and 1394 cm^{-1} in DEP-d_6, in good agreement with the experimental results (Tables 2 and 5). Accordingly, these CH_2 deformations are not affected appreciably by methyl deuteration. The corresponding CD_2 modes in DEP-d_4 are observed (calculated) at 1068 (1080) and 1169 (1198) cm^{-1}. The apparent reversal of frequencies in DEP-d_4, i.e., the CD_2 wagging mode is of higher frequency, can be attributed to mixing with both C—C and C—O stretching modes (Table 4). A similar reversal is predicted by ab initio calculation (Shaw et al., 1990; Guan and Thomas, 1996b).

TABLE 7 Molecular force fields of diethyl phosphate and dimethyl phosphate

Force constants	DEP		DMP	
	Ab initio	GVFF	Ab initio	GVFF
Stretching (mydn Å^{-1})				
1 P–O	8.529	8.721	8.527	8.541
2 P—O	5.342	4.627	5.353	4.928
3 C—O	4.276	4.532	4.635	4.693
4 C-H(CH_2)	4.730*	4.710		
5 C—C	4.210	4.366		
6 C-H(CH_3)	4.890*	4.823	4.934*	4.953
Bending (mdyn Å rad^{-2})				
7 O–P–O	0.876	1.510	0.887	1.510
8 O–P—O	1.207, 1.281	1.446	1.208, 1.292	1.446
9 O—P—O	1.312	1.490	1.320	1.490
10 P—O—C	0.699	0.705	0.716	0.705
11 O—C-H	0.682	0.835	0.664	0.879
12 O—C—C	0.919	1.182		
13 H-C-H(CH_2)	0.496	0.473		
14 H-C—C(CH_2)	0.566*	0.645		
15 C—C-H(CH_3)	0.530*	0.535		
16 H-C-H(CH_3)	0.453*	0.446	0.477*	0.572
Torsion (mdyn Å rad^{-2})				
17 O—P—O—C	0.093	0.080	0.096	0.080
18 P—O—C—C	0.038	0.038	0.032	0.038
19 O—C—C-H	0.112	0.025		
Stretching/stretching (mdyn Å^{-1})				
20 O–P/P–O	0.191	0.755	0.195	0.725
21 O–P/P—O	0.322, 0.286	0.516	0.321, 0.284	0.673
22 O—P/P—O	0.404	0.384	0.400	0.316
23 P—O/O—C	0.144	0.075	0.123	0.094
24 O—C/C-H(CH_2)	0.163*	0.260	0.162*	0.555
25 O—C/C—C	0.208	0.318		
26 H-C(CH_2)/C-H(CH_2)	0.065	0.043		
27 H-C(CH_2)/C—C	0.072	0.070		
28 C—C/C-H(CH_3)	0.060*	0.096		
29 H-C(CH_3)/C-H(CH_3)	0.055*	0.055	0.061	0.005
30 C—O/C—O	0.020	0.108	0.020	0.108
Bending/bending (mdyn Å rad^{-2})				
31 O–P–O/O–P—O	−0.170, −0.205	0.264	−0.170, −0.208	0.264
32 O–P–O/O—P—O	−0.399	0.130	−0.402	0.264
33 O–P—O/O–P—O	−0.352	−0.190	−0.350	
34 O–P—O/O–P—O	−0.060	−0.069	−0.063	
35 O–P—O/O—P–O	−0.538, −0.489	−0.383	−0.544, 0.487	
36 O–P—O/O—P—O	−0.141, 0.121	0.264	−0.142, −0.112	
37 O–P—O/P—O—C	−0.061, 0.017	0.0	0.057, 0.015	
38 O—P—O/P—O—C	−0.017	0.0	−0.020	
39 O—C-H(CH_2)/O—C-H(CH_2)	−0.144	−0.052		
40 O—C-H/O—C—C	−0.196	−0.200		
41 O—C-H/H-C-H(CH_2)	−0.086	−0.056		
42 O—C-H/H-C—C	−0.083, −0.156	0.031		
43 O—C-H/H-C—C	−0.153	−0.087		
44 O—C—C/H-C—C	−0.166	−0.131		
45 O—C—C/C—C-H(CH_3)#	−0.075	0.128		
46 H-C-H(CH_2)/H-C—C(CH_2)	−0.072	−0.070		
47 H-C—C(CH_2)/H-C—C(CH_2)	−0.106	−0.033		
48 H-C—C(CH_2)/C—C-H(CH_3)#	0.047	0.099		
49 C—C-H(CH_3)/C—C-H(CH_3)	−0.130*	−0.080	−0.162*	0.043
50 C—C-H(CH_3)/H-C-H(CH_3)	−0.094	−0.072		
51 H-C-H(CH_3)/H-C-H(CH_3)	−0.080*	−0.065	−0.072*	−0.013
52 O—C—C/C—C-H(CH_3)§	0.142	−0.044		
53 H-C—C(CH_2)/C—C-H(CH_3)§	0.105	−0.047		
Stretching/bending (mydn rad^{-1})				
54 O–P/O–P–O	0.088	0.357	0.087	0.357
55 O–P/O–P—O	0.127, 0.206	0.357	0.125, 0.205	0.359
56 P—O/O–P—O	0.289, 0.218	0.378	0.284, 0.220	0.378
57 P—O/O—P—O	0.287	0.380	0.287	0.380

TABLE 7 (*Continued*)

Force constants	DEP		DMP	
	Ab initio	GVFF	Ab initio	GVFF
Stretching/bending (mdyn rad^{-1}) *Continued*				
58 P—O/P—O—C	0.359	0.184	0.370	0.184
59 O—C/P—O—C	0.415	0.073	0.452	0.173
60 O—C/O—C-H	0.220*	0.226	0.225	0.441
61 O—C/O—C—C	0.275	0.597		
62 C-H/O—C-H	0.033	0.034	0.031, −0.055	0.214
63 C-H(CH_2)/H-C-H(CH_2)	0.090	0.140		
64 C-H/H-C—C(CH_2)	−0.090, 0.042	0.080		
65 C—C/O—C—C	0.139	0.137		
66 C—C/H-C—C(CH_2)	0.133	0.133		
67 C—C/C—C-H(CH_3)	0.120	0.117		
68 C-H(CH_3)/C—C-H(CH_3)	0.080	0.070		
69 C-H(CH_3)/H-C-H(CH_3)	0.082	−0.040		
70 P-O/O-P—O	−0.162	0.357	−0.161	
71 P-O/O—P—O	−0.152	0.359	−0.150	
72 P—O/O-P-O	−0.195	0.378	−0.197	
73 P—O/O—P-O	−0.220, −0.268	0.184	−0.216, −0.267	
74 O—C/H-C-H(CH_2)	−0.210	0.173		
75 O—C/H-C—C(CH_2)	−0.241, −0.236	0.441		
76 C-H(CH_2)/O—C-H(CH_2)	−0.049	0.214		
77 C-H(CH_2)/O—C—C	−0.050	0.340		
78 C-H(CH_2)/H-C—C(CH_2)	−0.076	0.340		
79 C—C/H-C-H(CH_2)	−0.149			
80 C—C/H-C—C(CH_3)	−0.124			
81 C-H(CH_3)/C—C-H(CH_3)	−0.083	0.214		
82 C-H(CH_3)/H-C-H(CH_3)	−0.079	0.214		
83 C—C/O—C-H(CH_2)	−0.132	−0.134		

Notation and abbreviations are given in Table 1.
*Average value.
#*Gauche* conformation.
§*Trans* conformation.

CH_3 deformation vibrations

Calculated deuteration shifts of methyl group vibrations (1450 → 1042, 1452 → 1040, and 1360 → 1128 cm^{-1}) are in good agreement with the data (Table 5). The 1450- and 1452-cm^{-1} frequencies, known as the pseudodegenerate CH_3 deformation modes, exhibit isotope shifts that are much larger than that of the 1360-cm^{-1} frequency (symmetric CH_3 deformation). The latter is explained by strong coupling between the symmetric CH_3 mode and the C—C stretching vibration and was discussed previously (Guan and Thomas, 1996b; Guan et al., 1994, 1995; Durig et al., 1991).

CH_3 and CH_2 rocking vibrations

The present calculations show that the perpendicular methyl rocking mode and methylene rocking mode are strongly coupled in DEP-h_{10}, to give frequencies at 1186 and 790 cm^{-1}. In DEP-d_4 (Table 4), DEP-d_6 (Table 5), and DEP-d_{10} (Table 6) the rocking modes are significantly shifted but remain coupled, though differently than in DEP-h_{10}. The normal coordinate calculations are in agreement with the frequencies and PED values obtained in previous ab initio calculations (Guan and Thomas, 1996b) and with experimental data (Table 2).

Generalized valence force field for DEP

The GVFF force constants are compared in Table 7 with scaled ab initio force constants of DEP and with corresponding values for DMP in Table 7. Overall, the GVFF and the ab initio force constants for stretching vibrations are in good agreement. An exception is the force constant for the P—O stretching vibration, which exhibits a GVFF value (4.627 mdyn Å^{-1}) that is ~15% smaller than the scaled ab initio value (5.342 mdyn Å^{-1}). A similar discrepancy occurs in DMP (Columns 4 and 5). As expected, force constants for bending agree only semiquantitatively because the valence force field is a limited subset of the comprehensive ab initio force field. Nevertheless, the GVFF for DEP reproduces satisfactorily the vibrational spectra of five DEP isotopomers and represents an improved approximation to the vibrational force field for the nucleic acid phosphate group.

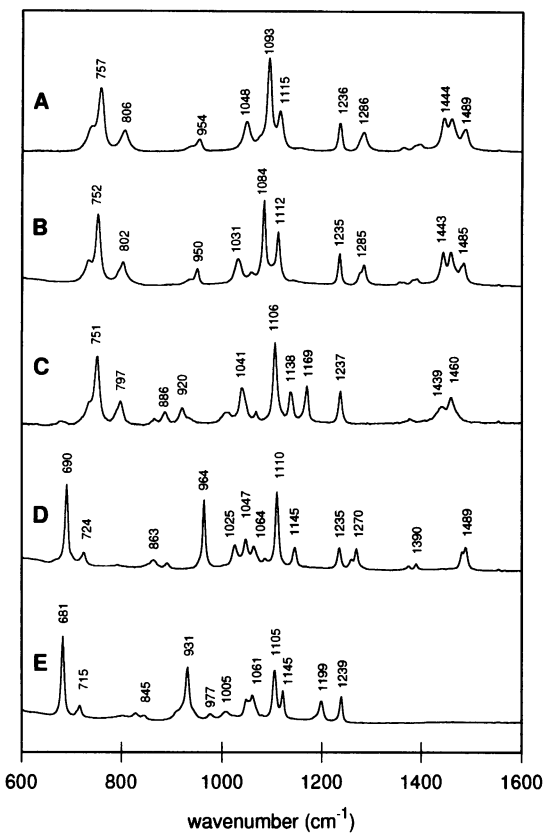

FIGURE 2 Raman spectra of barium salts of DEP isotopomers. (*A*) DEP-h_{10}, (*B*) DEP-$^{13}C_2$, (*C*) DEP-d_4, (*D*) DEP-d_6, (*E*) DEP-d_{10}. Spectra were excited at 514.5 nm on powder samples at 25°C.

Comparison of force fields of DEP and DMP

Table 7 shows that the scaled ab initio force constants for stretching and bending vibrations of PO_2^- and OPO groups of the O—P(O_2^-)—O moieties in DEP (column 2) and in DMP (column 4) are in good agreement. This agreement reflects their identical optimized structures (Guan et al., 1995; Guan and Thomas, 1996b). Conversely, the large difference (8%) in ab initio force constants for C—O stretching vibrations of the two structures (4.276 mdyn $Å^{-1}$ in DEP compared with 4.635 mdyn $Å^{-1}$ in DMP) presumably reflects the effects of different alkyl substituents on the stiffness of the C—O bond.

As expected, GVFF force constants of DEP and DMP (Table 7, columns 3 and 5) reveal greater discrepancies. Most significant is the force constant for P—O stretching, which diminishes from 4.928 mdyn $Å^{-1}$ in DMP to 4.627 mdyn $Å^{-1}$ in DEP (7%). A similar depression of this term has been reported by Taga et al. (1991).

Conformational dependence of DEP vibrations

Here we focus on the conformational dependence of symmetric and antisymmetric stretching vibrations of PO_2^-, OPO, C—O, and C—C groups. The sensitivity of the vibrational frequencies to changes in pairs of torsion angles, α and ζ or α and β, is shown in Figs. 3–6.

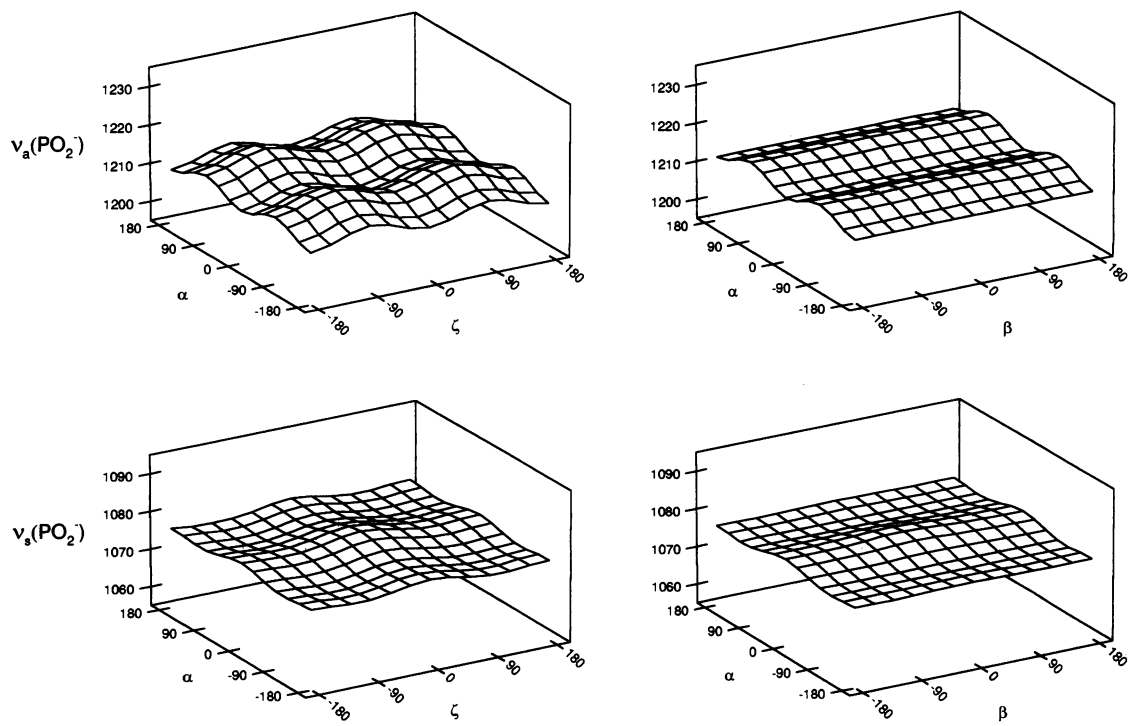

FIGURE 3 Conformational dependence of PO_2^- antisymmetric (*top*) and symmetric (*bottom*) stretching modes. (*Left*) Dependence on P—O torsion angles, $\tau 51(\alpha)$ and $\tau 52(\zeta)$, as defined in Fig. 1. C—O torsion angles, $\tau 53(\beta)$ and $\tau 55(\epsilon)$, are maintained in the *trans* conformation, and P—O torsions are varied. (*Right*) Interdependence of P—O and C—O torsions. Here torsions of one P—O—C group are maintained in the *gauche* and *trans* conformations, respectively, whereas those of the other P—O—C group are varied. Horizontal and vertical axes are in units of degrees and wavenumbers, respectively.

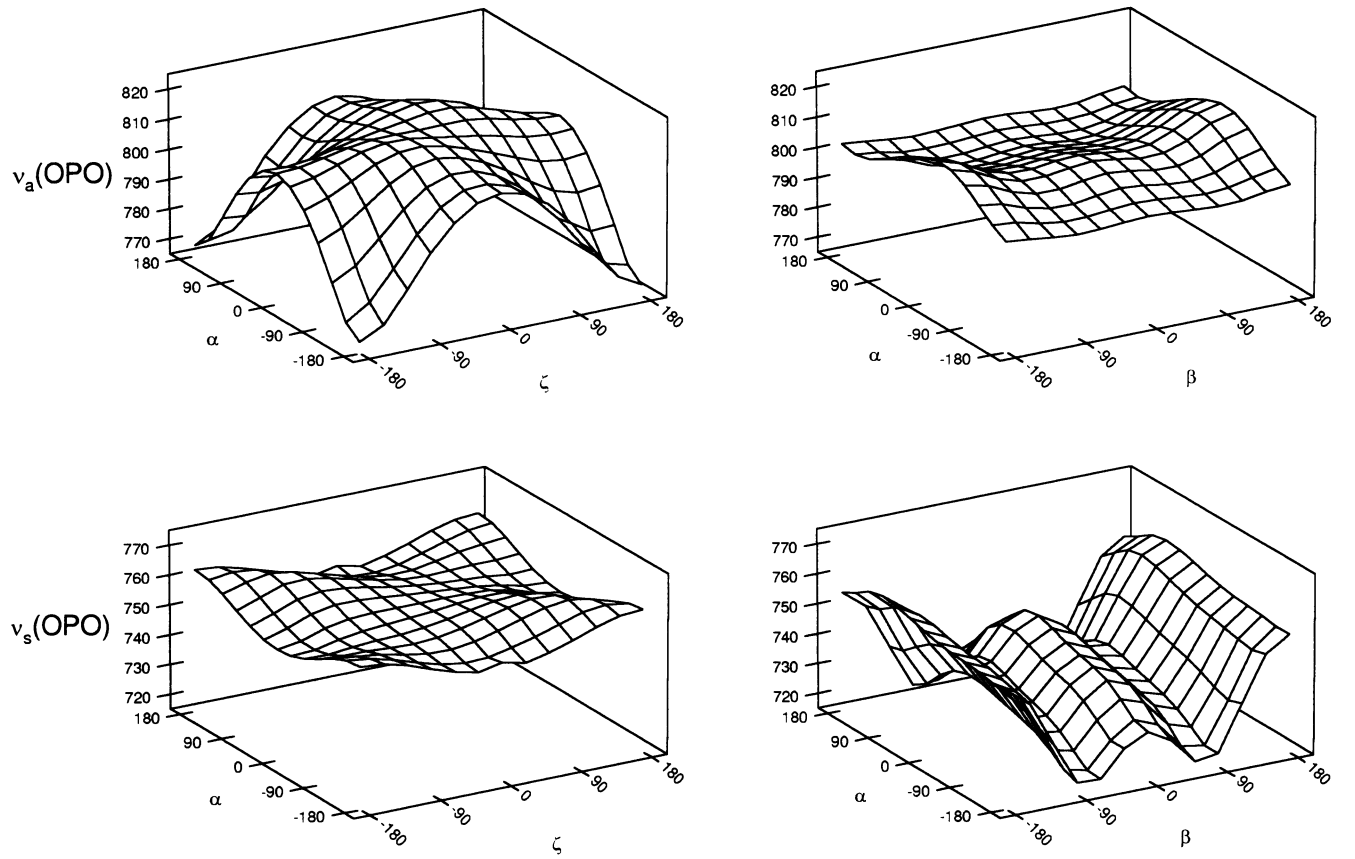

FIGURE 4 Conformational dependence of OPO antisymmetric (*top*) and symmetric (*bottom*) stretching modes. (*Left*) Dependence on P—O torsion angles, $\tau 51(\alpha)$ and $\tau 52(\zeta)$. (*Right*) Interdependence of P—O and C—O torsions. Further details and nomenclature are as described in Fig. 3.

PO_2^- stretching modes

Fig. 3 shows that antisymmetric (ν_a) and symmetric (ν_s) stretching modes of the PO_2^- group are virtually unshifted ($\delta \approx 0$ cm^{-1}) by changes in C—O torsion angles and are only marginally shifted ($\delta < 8$ cm^{-1}) by changes in P—O torsion angles. With both α and ζ at $\pm 90°$, ν_a achieves its maximum value (1217 cm^{-1}) and ν_s its minimum value (1075 cm^{-1}). On the other hand, ν_a is minimized (1209 cm^{-1}) and ν_s maximized (1080 cm^{-1}) when either torsion is 0° or ± 180°. These results are consistent with previous calculations for DEP (Bicknell-Brown et al., 1982; Taga et al., 1991) and DMP (Guan and Thomas, 1996a)

OPO stretching modes

Fig. 4 shows that the frequency of the antisymmetric stretching mode, ν_a(OPO), is strongly dependent on the P—O torsion angles. It is highest (814 cm^{-1}) when α and ζ are 0° and lowest (769 cm^{-1}) when α and ζ are 180°. However, ν_a(OPO) is not highly dependent on the C—O torsion angles. Conversely, the corresponding symmetric mode, ν_s(OPO), is more sensitive to C—O than to P—O torsions (bottom), exhibiting its minimum (719 cm^{-1}) and maximum (759 cm^{-1}) values with $\beta = \pm 90°$ and $\beta = 180°$, respectively. The present calculations are consistent with previous results for DEP (Taga et al., 1991) and DMP (Guan and Thomas, 1996a) and with empirically proposed spectra-structure correlations (Thomas and Wang, 1988; Thomas and Tsuboi, 1993). Importantly, they extend the previously demonstrated conformational dependencies of ν_a(OPO) and ν_s(OPO) (Guan and Thomas, 1996a) to include C—O as well P—O torsion angles.

C—O stretching modes

As shown in Fig. 5, the antisymmetric C—O stretching mode, ν_a(C—O), is appreciably dependent on C—O torsion angles, whereas the corresponding symmetric mode, ν_s(C—O), is less so. This situation is reversed for the P—O torsion angles.

C—C stretching mode

Fig. 6 shows that all C—C stretching modes depend to some extent on the skeletal torsion angles. This more complex conformation-dependent behavior may reflect the more ex-

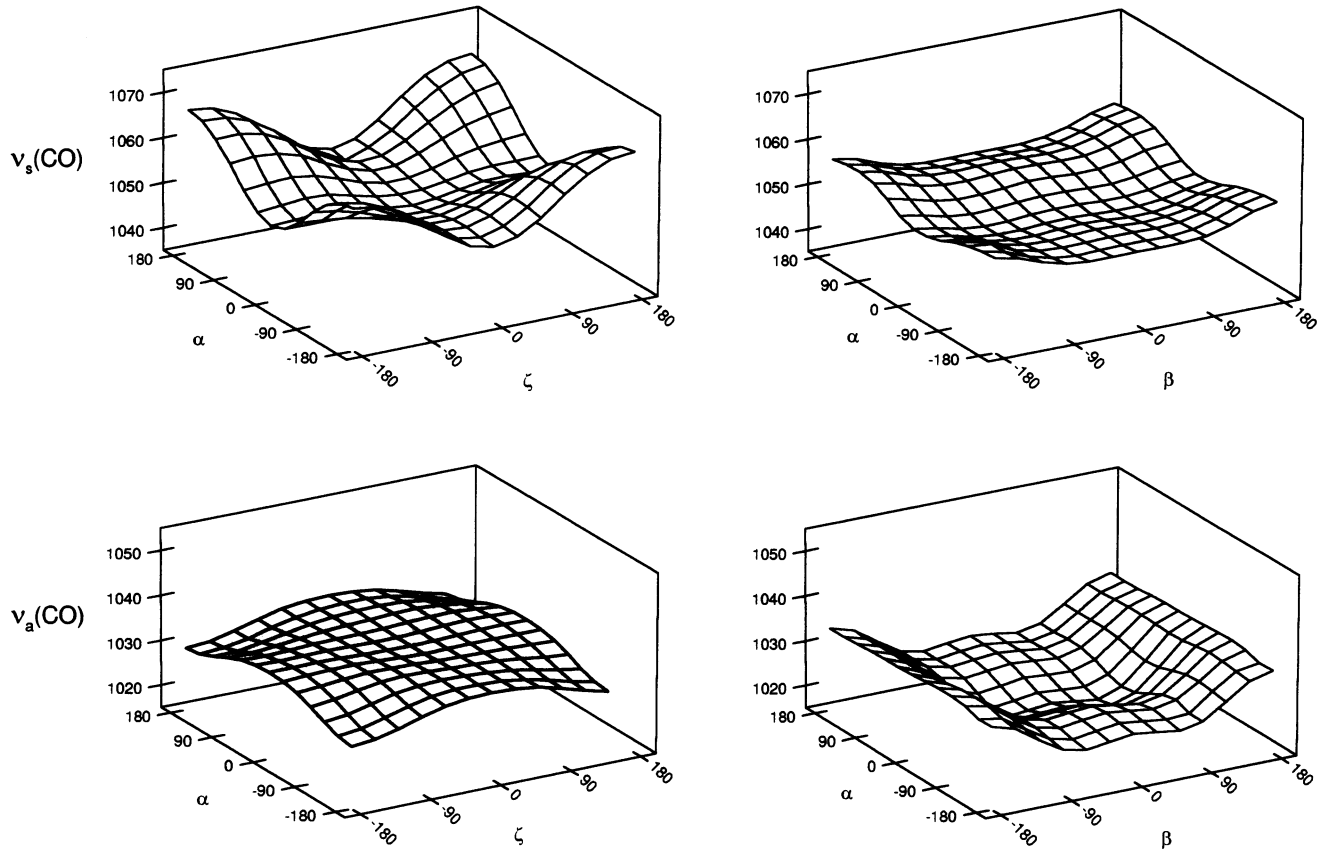

FIGURE 5 Conformational dependence of C—O symmetric (*top*) and antisymmetric (*bottom*) stretching modes. (*Left*) Dependence on P—O torsion angles, $\tau 51(\alpha)$ and $\tau 52(\zeta)$. (*Right*) Interdependence of P—O and C—O torsions. Further details and nomenclature are as described in Fig. 3.

tensive coupling of C—C stretching with other stretching modes of the diester network and with methyl rocking (Table 5).

CONCLUSIONS

To develop an improved understanding of the normal coordinates associated with conformation-dependent vibrational modes of the nucleic acid backbone, particularly those localized in the phosphodiester skeletal network, we have extended earlier normal coordinate calculations for dimethyl phosphate (DMP) to diethyl phosphate (DEP) and its ^{2}H and ^{13}C isotopomers. The DEP skeleton serves as an improved structural analog of the nucleic acid phosphate group and is expected to provide better insight into the nature of nucleic acid backbone vibrations, which are employed as empirical markers of DNA and RNA secondary structures. The infrared and Raman spectra collected on DEP isotopomers and reported here have served as the primary basis for refining the generalized valence force field of the C—C—O—P(O_2^-)—O—C—C network. We have also exploited the force field to assess the dependence of C—C, C—O, and P—O stretching vibrations on torsion angles corresponding to those (α, β, ϵ, and ζ) of the nucleic acid backbone. The principal conclusions derived from the present study are as follows:

1) The proposed generalized valence force field (GVFF) accurately reproduces the vibrational infrared and Raman spectra obtained on five DEP isotopomers.

2) The GVFF of DEP shows good agreement with the scaled ab initio force field reported previously (Guan and Thomas, 1996b).

3) The GVFF force constants for vibrations localized in the orthophosphate moiety (O—P(O_2^-)—O) of DEP are virtually identical to those of DMP. It is expected that these force constants will also be transferable to larger and more complex phosphodiester moieties, including the sugar phosphates of nucleic acids.

4) The GVFF frequencies for stretching vibrations localized in the P—O, C—O, and C—C bonds are generally sensitive to P—O and C—O torsion angles. Although the present approach is based on the approximation that force constants (**F**-matrix elements) are invariant to changes in skeletal torsion angles, i.e., the computed frequency dependencies of Figs. 3–6 are attributed solely to changes in molecular geometry (**G**-matrix elements), the results provide a starting point for understanding relationships between conformation-dependent vibrational modes and inter-

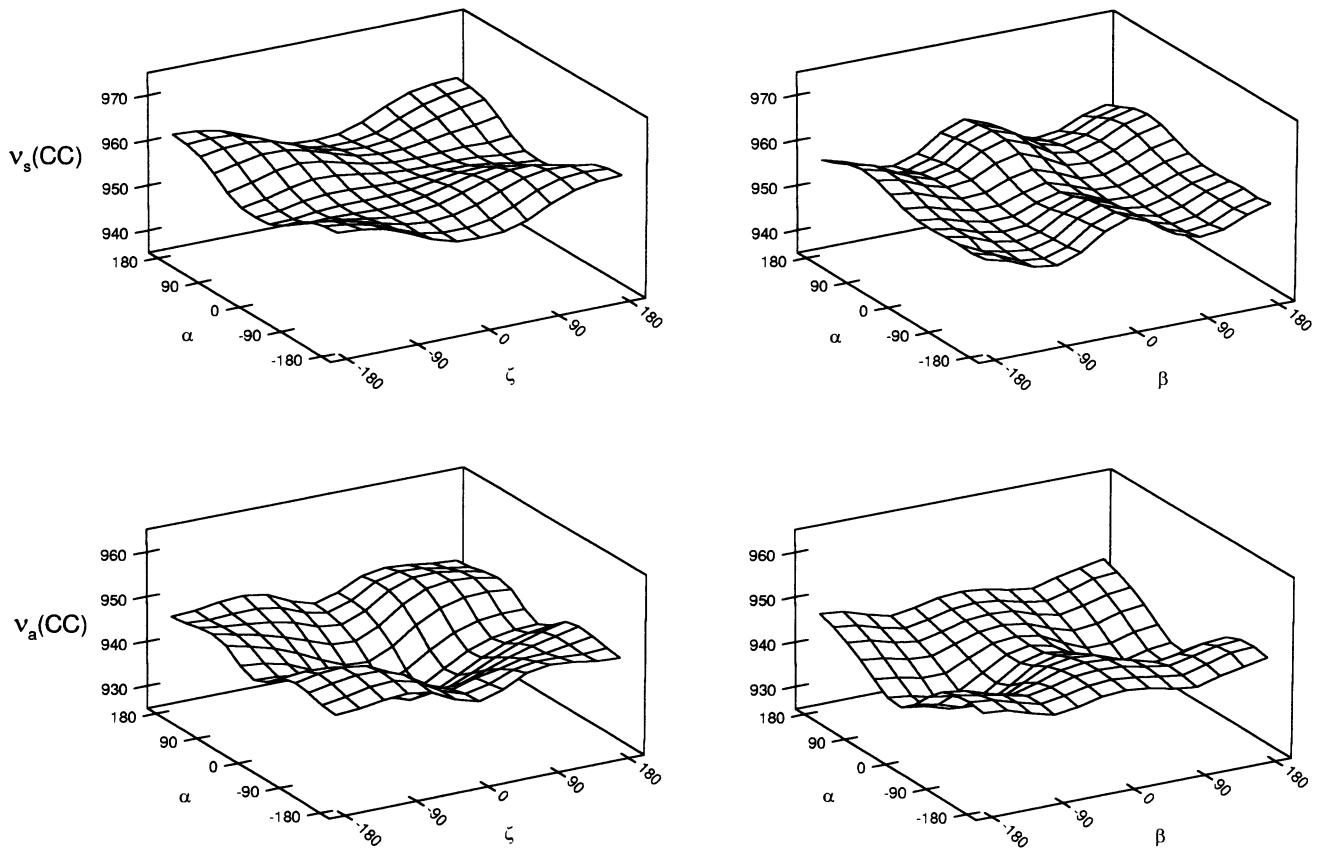

FIGURE 6 Conformational dependence of C—C symmetric (*top*) and antisymmetric (*bottom*) stretching modes. (*Left*) Dependence on P—O torsion angles, $\tau 51(\alpha)$ and $\tau 52(\zeta)$. (*Right*) Interdependence of P—O and C—O torsions. Further details and nomenclature are as described in Fig. 3.

nal coordinates of the nucleic acid backbone. Specifically, we find that phosphodiester stretching vibrations are the most highly sensitive to conformational change, with the symmetric and antisymmetric modes dependent, respectively, on C—O and P—O torsions. Tentatively, we propose the internal coordinate versus frequency correlations of Fig. 4 as an initial basis for understanding the conformation-dependent vibrations of nucleic acids in the region 750–875 cm^{-1} of Raman (Thomas and Tsuboi, 1993) and infrared spectra (Taillandier and Liquier, 1992).

5) The present GVFF accurately predicts the relative insensitivity of the symmetric phosphodioxy (PO_2^-) stretching vibration to changes in nucleic acid backbone geometry. This is in accord with the observation that the Raman band in question, which is centered near 1095 ± 5 cm^{-1} in all natural and synthetic nucleic acids, is minimally affected in frequency and intensity by a wide range of conformational perturbations to DNA and RNA (Thomas et al., 1971; Erfurth et al., 1972, 1975; Prescott et al., 1984; Duguid et al., 1996). The present calculations support previously proposed Raman spectra-structure correlations (Thomas and Wang, 1988; Thomas and Tsuboi, 1993).

6) Many of the vibrational modes observed in the 850-1050-cm^{-1} interval of nucleic acid Raman spectra have not yet been assigned with confidence. Empirical correlations are also largely unavailable. The situation is compounded by the fact that most of the spectral bands of this region are relatively weak, broad, and mutually overlapped. Nevertheless, Raman tensor determinations provide a basis for gaining an improved understanding of the nature of these vibrations in DNA duplexes (Thomas et al., 1995). A recent study of the Raman signature of the four-stranded intercalated cytosine motif (*i* motif) confirms that the 850-1050-cm^{-1} region is also highly sensitive to other types of secondary structure (Benevides et al., 1996). The present analysis demonstrates that coupled C—C and C—O stretching vibrations are the major contributors to bands between 850 and 1050 cm^{-1}. Additionally, appreciable coupling with P—O stretching and deformation modes is expected (Tables 2–6). The conformation-dependent behavior of these bands is therefore, not surprisingly, more complex than that of the more localized phosphodiester modes that occur below 850 cm^{-1}, as is evident from comparison of Figs. 4–6.

It is also appropriate to consider the limitations of the present model compound analysis. The phosphodiester marker band of a double-stranded DNA molecule of given base composition, such as calf thymus DNA, is highly sensitive to conformation, typically exhibiting a shift from 834 cm^{-1} in the *B* form to 807 cm^{-1} in the *A* form (Erfurth

et al., 1972; Prescott et al., 1984). Vibrational analysis of DEP provides only a qualitative basis for interpreting this effect. Additionally, *B*-form structures of different base composition exhibit clear-cut differences in the positions of phosphodiester marker bands. A definitive example of the latter phenomenon is the occurrence of the *B*-form marker at 829 cm^{-1} in poly(dG-dC)·poly(dG-dC) and at 839 cm^{-1} in poly(dA-dT)·poly(dA-dT). The 10 cm^{-1} spectral difference has been attributed to different local backbone geometries (Thomas et al., 1986). Thus, the present vibrational analysis can provide only a first approximation to understanding the conformation-dependent behavior of backbone vibrations of nucleic acids. Extension to more sophisticated models of the phosphodiester group is required. An obvious candidate for further study is a nonsymmetric diester, such as ethyl isopropyl phosphate, which should better simulate the C5′– and C3′–sugar linkages of DNA.

Support of this research by National Institutes of Health Grant GM54378 is gratefully acknowledged. We also thank Dr. Charles J. Wurrey (Department of Chemistry, University of Missouri, Kansas City, MO 64110) for helpful discussions and comments on the manuscript.

This is paper LXIII in the series Raman Spectral Studies of Nucleic Acids, supported by National Institutes of Health Grant GM54378.

REFERENCES

Benevides, J. M., C. Kang, and G. J. Thomas, Jr. 1996. Raman signature of the four-stranded intercalated cytosine motif in crystal and solution structures of DNA deoxycytidylates d(CCCT) and d(C_8). *Biochemistry.* 35:5747–5755.

Benevides, J. M., M. Tsuboi, A. H.-J. Wang, and G. J. Thomas, Jr. 1993. Local Raman tensors of double-helical DNA in the crystal: a basis for determining DNA residues orientations. *J. Am. Chem. Soc.* 115: 5351–5359.

Bicknell-Brown, E., K. G. Brown, and W. B. Person. 1982. Conformation-dependent Raman bands of phospholipid surfaces. 3. Head group orthophosphate stretching vibrations. *J. Raman Spectrosc.* 12:180–189.

Duguid, J. G., V. A. Bloomfield, J. M. Benevides, and G. J. Thomas, Jr. 1996. DNA melting investigated by differential scanning calorimetry and Raman spectroscopy. *Biophys. J.* In press.

Durig, J. R., H. Nanaie, and G. A. Guirgis. 1991. Raman and infrared spectra, barriers to internal rotation, vibrational assignments and ab initio calculations on 2-fluoropropane. *J. Raman Spectrosc.* 22:155–168.

Erfurth, S. C., P. J. Bond, and W. L. Peticolas. 1975. Characterization of the $A \leftrightarrow B$ transition of DNA in fibers and gels by laser Raman spectroscopy. *Biopolymers.* 14:1245–1257.

Erfurth, S. C., E. J. Kiser, and W. L. Peticolas. 1972. Determination of the backbone structure of nucleic acids and nucleic acid oligomers by laser Raman scattering. *Proc. Natl. Acad. Sci. USA.* 69:938–941.

Guan, Y., G. Choi, R. Glaser, and G. J. Thomas, Jr. 1995. Vibrational analysis of nucleic acids. 2. Ab initio calculation of the molecular force field and normal modes of dimethyl phosphate. *J. Phys. Chem.* 99: 12,054–12,062.

Guan, Y., and G. J. Thomas, Jr. 1996a. Vibrational analysis of nucleic acids. 3. Conformation-dependent Raman markers of the phosphodiester backbone modeled by dimethyl phosphate. *J. Mol. Struct.* 379:31–41.

Guan, Y., and G. J. Thomas, Jr. 1996b. Vibrational analysis of nucleic acids. 4. Normal modes of the DNA phosphodiester structure modeled by diethyl phosphate. *Biopolymers.* (in press).

Guan, Y., C. J. Wurrey, and G. J. Thomas, Jr. 1994. Vibrational analysis of nucleic acids. 1. The phosphodiester group in dimethyl phosphate model compounds: $(CH_3O)_2PO_2^-$, $(CD_3O)_2PO_2^-$, and $(^{13}CH_3O)_2PO_2^-$. *Biophys. J.* 66:225–235.

Hadzi, D., M. Hodoscek, J. Grdadolnik, and F. Avbelj. 1992. Intermolecular effects on phosphate frequencies in phospholipids - infrared study and ab initio model calculation. *J. Mol. Struct.* 266:9–19.

Kyogoku, Y., and Y. Iitaka. 1964. The crystal structure of barium diethyl phosphate. *Acta Crystallogr.* 21:49–57.

Liang, C., C. S. Ewig, T. R. Stouch, and A. T. Hagler. 1993. Ab initio studies of lipid model species. 1. Dimethyl phosphate and methyl propyl phosphate anions. *J. Am. Chem. Soc.* 115:1537–1545.

Prescott, B., W. Steinmetz, and G. J. Thomas, Jr. 1984. Characterization of DNA structures by laser Raman spectroscopy. *Biopolymers.* 23: 235–256.

Shaw, R. A., H. Wieser, R. Dutler, and A. Rauk. 1990. Vibrational optical activity of *(S)-1-d*-ethanol. *J. Am. Chem. Soc.* 112:5401–5410.

Snyder, R. G., and G. Zerbi. 1957. Vibrational analysis of ten simple aliphatic ethers: spectra, assignments, valence force field and molecular conformations. *Spectrochim. Acta.* 23A:391–437.

Taga, K., K. Miyagai, N. Hirabayashi, T. Yoshida, and H. Okabayashi. 1991. Vibrational spectra and normal coordinate analysis of barium dimethyl, diethyl and ethyl methyl phosphates. *J. Mol. Struct.* 245:1–11.

Taillandier, E., and J. Liquier. 1992. Infrared spectroscopy of DNA. *Methods Enzymol.* 211:307–335.

Terpstra, P. A., C. Otto, G. M. J. Segers-Nolten, J. S. Kanger, and J. Greve. 1995. Raman depolarization ratios in RNA and DNA are sensitive for sugar-base coupling. *Biospectroscopy.* 1:255–263.

Thomas, G. J., Jr., J. M. Benevides, S. A. Overman, T. Ueda, K. Ushizawa, M. Saitoh, and M. Tsuboi. 1995. Polarized Raman spectra of oriented fibers of *A* DNA and *B* DNA: anisotropic and isotropic local Raman tensors of base and backbone vibrations. *Biophys. J.* 69:1073–1088.

Thomas, G. J., Jr., J. M. Benevides, and B. Prescott. 1986. DNA and RNA structure in crystals, fibers and solutions by Raman spectroscopy with applications to nucleoproteins. *Biomol. Stereodynam.* 4:227–253.

Thomas, G. J., Jr., G. C. Medeiros, and K. A. Hartman. 1971. The dependence of Raman scattering on the conformation of ribosomal RNA. *Biochem. Biophys. Res. Commun.* 44:587–592.

Thomas, G. J., Jr., and M. Tsuboi. 1993. Raman spectroscopy of nucleic acids and their complexes. *Adv. Biophys. Chem.* 3:1–70.

Thomas, G. J., Jr., and A. H.-J. Wang. 1988. Laser Raman spectroscopy of nucleic acids. *In* Nucleic Acids and Molecular Biology, Vol. 2. F. Eckstein and D. M. J. Lilley, editors. Springer-Verlag, Berlin. 1–30.

Wilson, E. B., Jr., J. C. Decius, and P. C. Cross. 1955. Molecular Vibrations. McGraw-Hill, New York.

Zhao, W., J. Bandekar, and S. Krimm, 1990. Vibrational studies of the disulfide group in proteins. 3. A simplified *ab initio* force field for diethyl disulfide and SS and CS stretch frequency-conformation correlations for diisobutyl disulfide. *J. Mol. Struct.* 238:43–54.